

Enhanced definition PET for cardiac imaging

Ludovic Le Meunier, PhD,^{a,c} Piotr J. Slomka, PhD,^{a,b} Damini Dey, PhD,^{a,b} Amit Ramesh, MSc,^b Louis E. J. Thomson, MBChB, FRACP,^a Sean W. Hayes, MD,^a John D. Friedman, MD,^a Victor Cheng, MD,^a Guido Germano, PhD,^{a,b} and Daniel S. Berman, MD^{a,b}

Background. We aimed to determine in phantom and cardiac clinical studies the impact of a new high-resolution PET image reconstruction.

Methods. A phantom with cardiac insert filled with ¹⁸F, 14 ¹⁸F-FDG viability studies and 15 ⁸²Rb perfusion studies were acquired on a Siemens Biograph-64 (4-ring). The data were reconstructed with 2D- and 3D-attenuation weighted ordered subsets expectation maximization (AWOSEM), and high-definition reconstruction (HD-PET). We calculated wall/cavity contrast, contrast-to-noise ratio (CNR), wall thickness, motion/thickening and ejection fraction.

Results. In the phantom study, we found an increase in defect size (up to 26%), contrast (up to 48%) and CNR (1.9) with HD-PET as compared to standard techniques. The contrast increased on HD-PET images compared to 2D- and 3D-AWOSEM for viability (14.0% ± 4.8%) and perfusion studies (7.3% ± 4.3%) ($P < .05$). Average CNR increased with HD-PET by 79.4% ± 17.1% and 68.8% ± 3.0% in viability and perfusion studies respectively (all $P < .05$). Average wall thickness with HD-PET decreased in the phantom study by 1.3 ± 0.3 mm and the viability studies by 1.9 ± 0.7 mm but not in the perfusion studies. The functional measurements were not significantly different for any techniques.

Conclusions. We demonstrated both in phantom and patient cardiac studies that HD-PET improves image contrast, defect definition, and CNR. (J Nucl Cardiol 2010;17:414–26.)

Key Words: High definition • PET/CT imaging • myocardial viability • ¹⁸F-FDG • ⁸²Rb

INTRODUCTION

Reconstruction techniques have an impact on image quality and quantitative analysis in cardiac PET. Recently, new high-resolution reconstruction techniques which take advantage of resolution recovery principles have been presented.^{1–4} In particular, high definition reconstruction for PET (HD-PET) has been introduced by Siemens Healthcare Molecular Imaging (Knoxville, TN).⁵ Unlike the classic reconstruction techniques, this new iterative reconstruction algorithm compensates for the distortions introduced in the final images by the

circular geometry of the scanner. The result is an image with improved spatial resolution and a better control of the noise.⁵

In this work, we hypothesized that HD-PET provides cardiac images with a higher technical quality and we aimed to verify this in a cardiac phantom and in patient images. We tested the impact of HD-PET on image contrast, noise and myocardium wall thickness. We compared HD-PET reconstruction to regular 2D and 3D reconstruction techniques used at our institution. Phantom experiments were performed with Fluorine-18 and patient images were obtained with Fluorine-18 fluorodeoxyglucose (¹⁸F-FDG)⁶ and perfusion studies were obtained using Rubidium-82.⁷ We show significant improvements in technical cardiac image quality with the use of the high-resolution reconstruction.

MATERIALS AND METHODS

PET Acquisition and Reconstruction

All images were acquired on a Siemens Biograph-64 TruePoint PET/CT with the TrueV option. This 3D system consists of a 64-slice CT and a PET scanner with 4 rings of

From the Departments of Imaging and Medicine,^a Cedars-Sinai Medical Center, Los Angeles, CA; Department of Medicine,^b David Geffen School of Medicine at UCLA, Los Angeles, CA; Siemens Healthcare Molecular Imaging,^c Knoxville, TN.

Received for publication Sep 12, 2009; final revision accepted Jan 25, 2010.

Reprint requests: Ludovic Le Meunier, PhD, Departments of Imaging and Medicine, Cedars-Sinai Medical Center, Taper Bldg, #A238, 8700 Beverly Blvd, Los Angeles, CA 90048, USA; ludovic.lemeunier@cshs.org.

1071-3581/\$34.00

Copyright © 2010 by the American Society of Nuclear Cardiology.

doi:10.1007/s12350-010-9193-7

lutetium oxyorthosilicate (LSO) detectors with a detector element dimensions of $4 \times 4 \times 20$ mm³.⁸ The image plane spacing is 2 mm. The PET axial and transaxial FOV are 216 and 605 mm, respectively. The coincidence time window and the energy window are respectively 4.5 ns and 425–650 keV. The data was acquired in list mode format. A full description of the system performance can be found in Townsend et al.⁹

HD-PET Reconstruction Principle

When a gamma photon is detected by a PET system, it has to travel a certain distance before the crystal converts its energy into light. A gamma photon coming from the center of the field of view is likely to be localized on the correct line of response (LOR). However, if the photon is emitted away from the center of the FOV, it strikes a crystal at an angle because of the circular geometry of the tomograph. In this case, the gamma photon is likely to continue traveling to the adjacent detector element. This results in an incorrect LOR and distortions in the final image. The probability that the photon is correctly localized decreases when the distance to the center of the FOV increases. These distortions have a negative impact on the spatial resolution and on the noise in the reconstructed images. See Figure 1 for the illustration of the problem.

A point spread function (PSF) describes the response of an imaging system to a point source in the FOV. The responses of a point source at given 3D locations of the FOV can be used to recover the original shape and form of the imaged object

(Figure 1). Those individual PSFs have been experimentally obtained in the factory for all 3D locations within the FOV for a given scanner model. While standard reconstruction assume the PSF to be the same everywhere in the FOV, HD-PET incorporates individually measured PSFs in the reconstruction process and then effectively localizes the photons on the right LORs. Consequently, the blurring and distortions in the final image are significantly reduced, leading to a better control of the noise and an improved more uniform spatial resolution.⁵

Phantom Experiments

We used a RSD Alderson Thorax phantom (Radiology Support Devices, Inc.) with cardiac insert to test the capabilities of HD-PET in cardiac imaging. We filled the myocardial wall and cavity respectively with 110 and 11 kBq/mL of ¹⁸F (Figure 2). We acquired the phantom images for 10 minutes and repeated this experiment with two cardiac defects in place (defect #1 volume: 13.5 mL; defect #2 volume: 41.7 mL). All the other acquisition parameters were set up to mimic patient acquisition (see below for details).

Patient Acquisition

We evaluated retrospectively ¹⁸F-FDG viability and ⁸²Rb perfusion patient studies performed for clinical indications. IRB was obtained for retrospective analysis of these data.

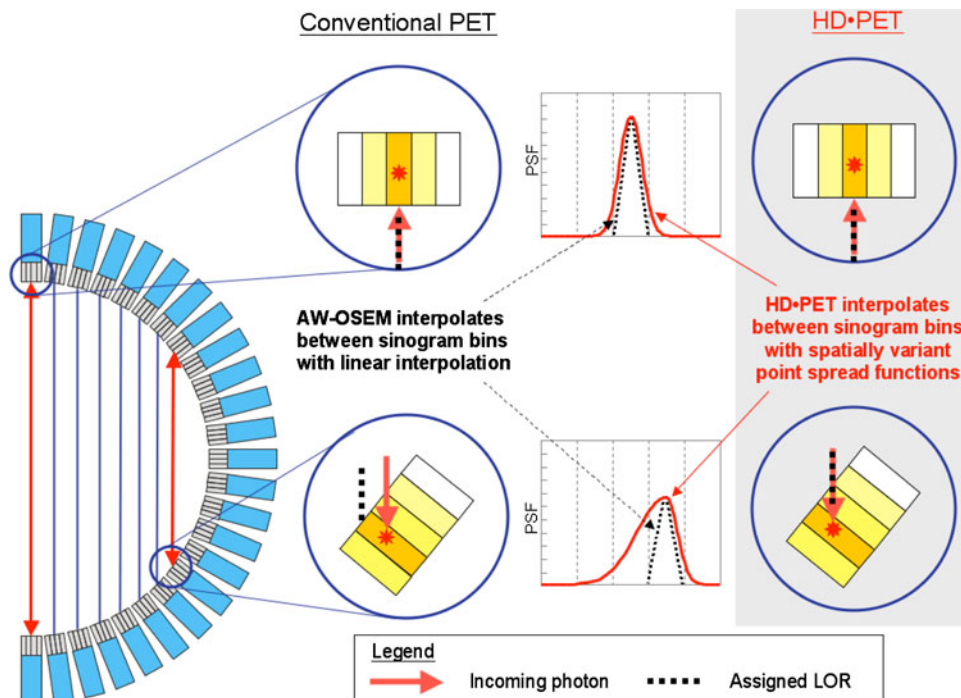


Figure 1. HD-PET principle. Due to the circular geometry of the tomograph, photons emitted off center of the field of view are incorrectly localized on the line of response creating image distortions in conventional PET (left). HD-PET (right) uses measured point spread functions (PSF; middle) to correct for those distortions consequently improving noise and spatial resolution in the reconstructed images.

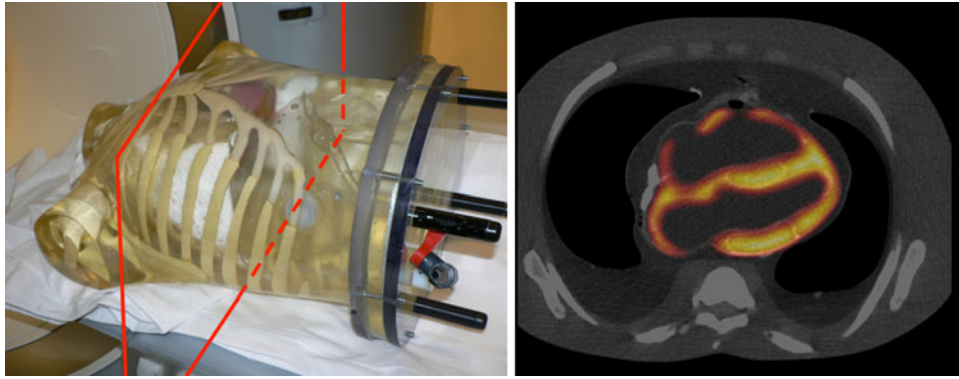


Figure 2. Photograph and PET/CT fusion image of ^{18}F filled RSD Alderson Thorax phantom (Radiology Devices, Inc.) with cardiac insert used in this study. The slice selected in the fusion image is materialized on the photograph.

^{18}F -FDG viability studies. The overall study population consisted of 14 consecutive patients (13 males and 1 female) referred for myocardial viability assessment. The average age of these patients was 66 ± 11 years, the average weight was 82 ± 13 kg (182 ± 28 lbs) (range 63-129 kg; 139-284 lbs), and the average body mass index (BMI) was 28.3 ± 5.9 (range 22.2-46.4).

After at least 4 hours of fasting, 370 MBq of ^{18}F -FDG was injected intravenously to all patients. A 60-minute uptake phase followed the injection. After a 2.8-second topogram acquisition (120 peak kilovoltage (kVp)), patients underwent a CT scan for attenuation correction (CTAC). The CT parameters were spiral mode, slice thickness 3.0 mm, total scan time 3.36 seconds, pitch 1.5, rotation time 0.5 seconds, collimation 24×1.2 mm, tube voltage 120 kVp, tube current 11 mAs and patient dose 0.74 mGy (0.3 mSv).

Subsequently, ^{18}F -FDG emission data were acquired for 1 bed position around the heart (216 mm coverage, identical to the CT protocol). ECG-gated 10-minute acquisition was performed in 3D and in list mode. During both the CT and the PET acquisitions, the patients were instructed to breathe normally.

^{82}Rb perfusion studies. The overall study population consisted of 15 consecutive patients (11 males, 4 females) who underwent a rest ^{82}Rb PET/CT scan which was part of a rest/stress study. The average age of these patients was 68 ± 15 years, the average weight was 76 ± 20 kg (167 ± 43 lbs) (range 47-103 kg; 104-227 lbs), and the average BMI was 25.3 ± 6.5 (range 13.6-37.4).

All patients underwent a rest/stress ^{82}Rb PET/CT study. Images were acquired in 3D and list mode with CT-based attenuation correction. Patients were studied after 24-hour abstinence from caffeinated drinks. Patients were instructed to perform normal breathing throughout the duration of the whole scan as reported in previous studies.⁷ A 2.8-second topogram acquisition with 120 peak kVp was followed immediately by the CT scan for AC. The CT acquisition parameters and breathing instructions were identical to the CT acquired for the viability studies.

Subsequently, rest PET images were acquired starting at the injection time. Typically, the injected dose was 30 mCi of ^{82}Rb for patients under 200 lbs, 40 mCi for patients between 200 and 250 lbs, and 50 mCi for patients over 250 lbs.

After completion of rest ^{82}Rb scan, patients underwent stress adenosine scan. However, stress images were not considered in this work since the misregistration between PET and CT due to breathing motion could introduce a bias in the results, as it is likely to be larger during the stress part of a ^{82}Rb perfusion study.

Reconstruction Protocols

Both phantom and patients emission data were reconstructed with the standard reconstruction technique used at our institution, 2D-attenuation weighted ordered subsets expectation maximization (AWOSEM). All data were also reconstructed with 3D-AWOSEM and HD-PET methods. The reconstruction matrix was $168 \times 168 \times 109$ with a zoom of 2 and the pixel size was $2 \times 2 \times 2$ mm³. Scatter correction, decay correction and random correction have been applied to the reconstructed images. The attenuation correction was CT-based. For ^{82}Rb perfusion images, prompt gamma correction was included in the scatter correction.¹⁰

For the phantom images, we used a number of maximum likelihood (ML) equivalent iterations (defined as the product of the number of iterations and the number of subsets) ranging from 8 to 112¹¹ to establish the optimal number of iterations (total of 11 reconstructions per iterative reconstruction techniques). No post-filtering, 3D 2-mm and 4-mm Gauss filtering (GF) were applied to the images.

For patients' studies, static and 8-bin ECG-gated images were generated with 2D-AWOSEM, 3D-AWOSEM and HD-PET after the sorting of the list file. Since the optimal spatial resolution with HD-PET was found to be 2 mm,⁵ we chose to filter all patient images with a 2-mm GF. Reconstruction parameters established during the phantom imaging were applied to patient studies. For the ^{82}Rb rest studies, the first two minutes of the list file were ignored to allow blood pool

clearance and the next three minutes of acquisition were used to generate sinograms. The number of iterations was chosen based on the phantom results. The quality of the registration between PET and CT was first estimated by experienced nuclear cardiology technologists using fused images in the Siemens 3D software on a Leonardo workstation (version Syngo 6.0). When a misalignment was identified, a manual registration matrix with 3D translations was generated by the technologists and applied before the final reconstruction process. Both the original CT-PET alignment and the alignment after manual registration were checked by the physicians. Manual CT-PET registration was performed in 3 cases out of the 14 viability patients and in 2 cases out of the 15 perfusion patients.

Image Analysis

Short-axis reorientation and automatic contouring of the left ventricle for phantom and patients' images were done automatically using QPET software (Cedars Sinai Cardiac Package) for which input were transverse slices of reconstructed PET images.¹² The myocardial wall segment analysis was done with the 17-segment American Heart Association (AHA) model.¹³

Myocardium to blood contrast and contrast-to-noise ratio. Volumes of interest (VOI) over the left ventricle and the blood pool (significantly larger than the spatial resolution in the image) were automatically derived based on the QPET segmentation of the left ventricle. We calculated the contrast (Cont) between the blood pool and the myocardial wall, and the contrast-to-noise (CNR) as follows:

$$\text{Cont} = \frac{\text{mean}(\text{Ventricular_VOI})}{\text{mean}(\text{Blood_VOI})}$$

$$\text{CNR} = \frac{\text{mean}(\text{Ventricular_VOI}) - \text{mean}(\text{Blood_VOI})}{\text{RMS_Noise}(\text{Blood_VOI})}$$

where RMS_Noise is the root mean square of the noise as defined by the standard deviation of the blood VOI. For the phantom, contrast and CNR have been obtained for all the reconstruction parameters studied. For the patients' studies, contrast and CNR were calculated from static summed images, globally and for each of the 17 AHA segments, and separately from all 8 gates. To provide optimal reconstruction parameters for each of the reconstruction techniques, we have first derived the optimal number of iterations for each technique for which maximal myocardial CNR was obtained in the phantom experiment.

Contrast between defect and maximum uptake in myocardium. We have calculated the contrast between the average of the closest neighbors around the minimum (27 voxels) in segments with defects, and the average of the closest neighbors (27 voxels) around the maximum of the myocardium. The segments with defects have been specified using the original physician report based on 2D-AWSEM images.

Phantom myocardial defect size. To test the effect of HD-PET reconstruction on myocardial defect quantification, we used Cedars-Sinai Cardiac QPET package, which includes direct change analysis and allowed us to compare the phantom acquisitions with and without defects, without the use of normal databases. The analysis method is based on a direct voxel-by-voxel subtraction of these images after iterative normalization of counts.¹⁴ The same left ventricular contours derived from the first scan (without defects) were used for datasets with and without defects (Figure 3). In this analysis, we used a 3% threshold change established empirically specifically for the phantom data, based on the count statistics and count variability in the myocardial phantom region without any defects.

Myocardial wall thickness and wall volume. Using the contours automatically detected by QPET, we estimated the myocardial wall volume for patients' studies and for all the reconstruction methods considered in this work. We also measured the wall thickness defined as the full-width half-maximum (FWHM) of a profile taken on the images at mid-long axis.

Ejection fraction, wall motion and wall thickening. The ejection fraction defined as the percentage difference between end-diastole and end-systole volumes automatically detected by QPET have been reported in this

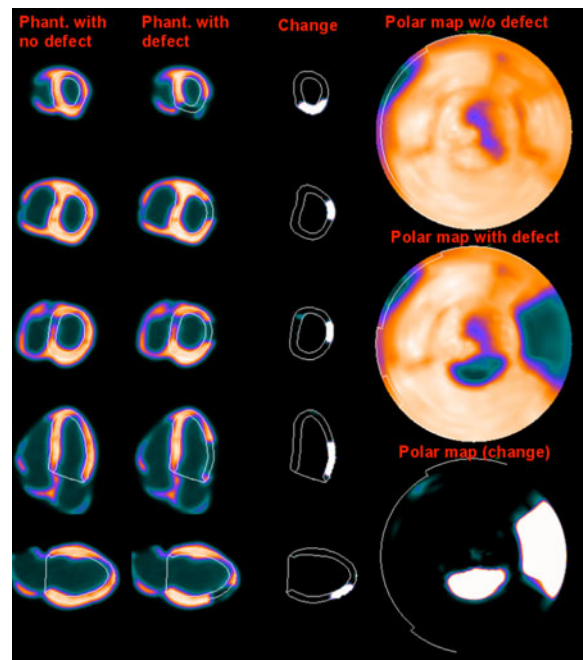


Figure 3. Defect quantification with Cedars-Sinai Cardiac Package. Short axis, vertical and horizontal axis view of the phantom without defect (*left*, first column), with defect (*left*, second column) and of the change between the two (*left*, third column). Corresponding polar maps are shown in the furthest column on the right. The volumes of the defects are 13.5 and 41.7 mL.

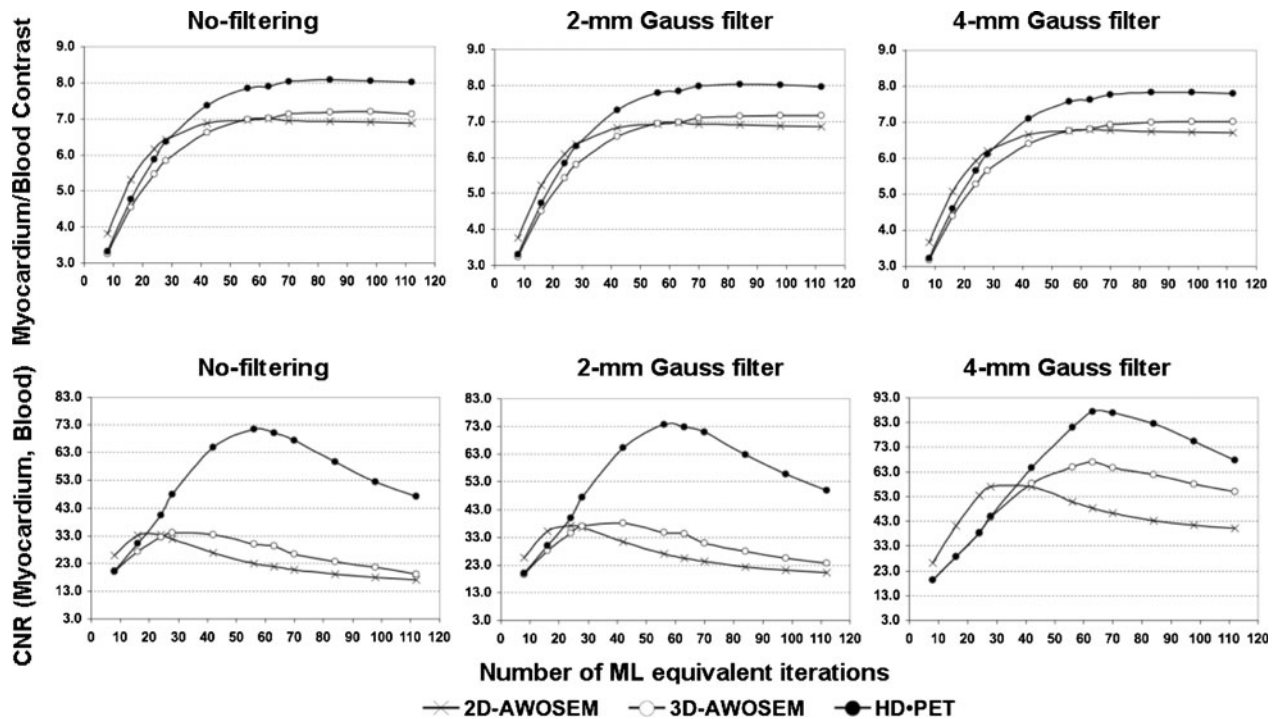


Figure 4. Myocardium/blood pool contrast (*top*) and CNR (*bottom*) on phantom images reconstructed with 2D- (*crosses*) and 3D-AWOSEM (*white dots*), and HD-PET (*black dots*) vs the number of ML equivalent iterations with no filtering (*left*), 2-mm (*middle*) and 4-mm Gauss filter (*right*).

work. QPET also provides us with global wall motion and global wall thickening and for each segment of the 17-segment AHA model used in this work. These algorithms have been recently optimized and validated for PET.¹⁵

Statistical Analysis

All continuous variables are expressed as mean \pm one standard deviation. Paired *t*-tests were used to compare differences in paired continuous data, and McNemar's tests were used to compare differences in paired discrete data. For unpaired continuous data, one-way ANOVA was used. All statistical tests were 2-tailed, and a value of $P < .05$ was considered significant.

RESULTS

Reconstruction Time

For all the reconstructions, we used Windows XP PC with two 2.33 GHz Intel Xeon processors. After the list mode sorting phase, the reconstruction time of the static images (matrix size $168 \times 168 \times 109$) was 1 minute 57 seconds for 2D-AWOSEM (3 iterations 8 subsets, 24 ML equivalent iterations), 1 minute 58 seconds for 3D-AWOSEM (3 iterations 14 subsets, 42 ML equivalent iterations) and 2 minutes 35 seconds for

HD-PET (4 iterations and 14 subsets, 56 ML equivalent iterations). The gated reconstruction time was 8 minutes 28 seconds for 2D-AWOSEM, 9 minutes 24 seconds for 3D-AWOSEM and 14 minutes 27 seconds for HD-PET.

Phantom Results

Contrast and contrast-to-noise ratio. In the phantom study with a 2-mm GF, we found that the highest myocardium-blood CNR with HD-PET was reached with 56 ML equivalent iterations (4 iterations and 14 subsets) vs 24 for 2D-AWOSEM (3 iterations and 8 subsets) and 42 for 3D-AWOSEM (3 iterations and 14 subsets). We found that the optimal number of iterations for HD-PET derived from our phantom study was in agreement with an optimization study recently published by Kadmas et al.¹⁶ Figure 4 shows the contrast and CNR vs the number of iterations for different filters for HD-PET and the two other reconstruction methods. Both contrast and CNR were increased with HD-PET compared to conventional reconstructions. The contrast increase between HD-PET and the conventional reconstruction methods ranged from +12.0% to +47.9% depending on the post-filtering (all $P < .05$). Table 1 shows the increases in contrast for HD-PET. Subsequently, the most optimal parameters providing highest

Table 1. Myocardial/blood contrast increase in phantom images reconstructed with HD-PET compared to 2D-AWOSEM and 3D-AWOSEM

HD-PET (56 ML ite.) vs	No-filter	2-mm Gauss filter	4-mm Gauss filter
2D-AWOSEM	+47.9% (16 ML ite.)	+28.0% (24 ML ite.)	+22.2% (28 ML ite.)
3D-AWOSEM	+34.3% (28 ML ite.)	+18.3% (42 ML ite.)	+12.0% (56 ML ite.)

Ite., Iterations.

CNR for each reconstruction technique were used for all further comparisons. Since the phantom results were similar for all three levels of filtering, we chose to apply the 2-mm GF to the rest of the phantom experiments and to the patient images.

Phantom myocardial wall thickness. We found that the wall thickness measured as the FWHM was 11.1 ± 0.6 mm for 2D-AWOSEM, 10.3 ± 0.7 mm for 3D-AWOSEM and 9.4 ± 0.3 mm for HD-PET. The HD-PET was the closest to the physical wall thickness of the phantom (9.0 mm).

Myocardial defect size. Relative defect size was higher for HD-PET as compared to other reconstructions. The estimated defect size went from 40.2 mL for 2D-AWOSEM and 43.2 mL for 3D-AWOSEM, to 49.2 mL for HD-PET. The global defect size was underestimated for all the reconstructions techniques; however, HD-PET was the closest to the real size in the phantom (55.2 mL).

Contrast between defect and maximum uptake in myocardium. We found that the maximum-to-defect contrast in the phantom was significantly improved with HD-PET (8.7 ± 0.2) as compared to 2D-AWOSEM (6.8 ± 1.4) and 3D-AWOSEM (7.0 ± 1.0).

Patient Results

All patient images have been reconstructed with reconstruction parameters optimized in the phantom experiments. We used 3 iterations and 8 subsets for 2D-AWOSEM (24 ML equivalent iterations), 3 iterations and 14 subsets for 3D-AWOSEM (42 ML equivalent iterations) and 4 iterations and 14 subsets for HD-PET (56 ML equivalent iterations).

Contrast and contrast-to-noise ratio. CNR and contrast were significantly increased with HD-PET for both ^{18}F -FDG and ^{82}Rb scans. The CNR for static viability (perfusion) images reconstructed with HD-PET was increased by 1.8 (1.6) compared to 2D-AWOSEM and 1.6 (1.6) compared to 3D-AWOSEM (all $P < .05$). The myocardial VOI on the static images showed an average contrast increase with HD-PET of $12.6\% \pm 6.8\%$ ($+4.5\% \pm 6.7\%$) and $17.6\% \pm 6.4\%$ ($+8.5\% \pm 2.6\%$) compared to 2D- and 3D-AWOSEM respectively (all $P < .05$). All results are summarized in Table 2. None of the segments show a change in contrast with HD-PET significantly different from any other segment, as shown by Bland-Altman analysis. Full results per segment are given in Table 3 (viability studies) and Table 4 (perfusion studies). Examples of the contrast

Table 2. ^{18}F -FDG viability and ^{82}Rb perfusion studies—CNR, contrast, maximum-to-defect contrast with HD-PET compared to 2D-AWOSEM and 3D-AWOSEM (static and gated reconstructions)

	CNR		Contrast		Max-to-defect contrast
	Static	Gated	Static	Gated	
^{18}F -FDG viability					
2D-AWOSEM	25.6 ± 13.0	10.3 ± 4.1	4.7 ± 1.8	4.5 ± 1.5	7.4 ± 4.0
3D-AWOSEM	27.7 ± 13.1	11.8 ± 5.4	4.4 ± 1.6	4.3 ± 1.4	7.3 ± 3.6
HD-PET	44.9 ± 21.0	20.9 ± 9.8	5.3 ± 2.1	4.9 ± 1.6	9.0 ± 4.8
^{82}Rb perfusion					
2D-AWOSEM	10.4 ± 4.4	4.1 ± 1.7	2.5 ± 0.5	2.5 ± 0.5	3.0 ± 0.7
3D-AWOSEM	10.7 ± 4.0	4.1 ± 1.5	2.4 ± 0.4	2.3 ± 0.4	2.9 ± 0.6
HD-PET	17.6 ± 5.9	7.0 ± 2.8	2.6 ± 0.5	2.6 ± 0.5	3.2 ± 0.7

We considered 64 segments with defect for viability patients and 25 segments with defect for perfusion patients. All $P < .05$.

Table 3. ¹⁸F-FDG viability studies

¹⁸ F viability segments	Average contrast			HD-PET vs 2D		HD-PET vs 3D	
	2D	3D	HD-PET	Lin. reg. (slope and r)	Bland-Altman (bias, 95%LOAs)	Lin. reg. (slope and r)	Bland-Altman (bias, 95%LOAs)
Basal							
1. Anterior	5.3 ± 1.9	5.1 ± 1.7	6.0 ± 2.1	1.1257 r = 0.9948	0.685 0.103-1.267	1.1849 r = 0.9885	0.911 -0.117 to 1.940
2. Anteroseptal	4.5 ± 2.3	4.2 ± 2.2	5.1 ± 2.7	1.1388 r = 0.9924	0.573 -0.456 to 1.602	1.2082 r = 0.9930	0.845 -0.348 to 2.037
3. Inferoseptal	4.5 ± 2.0	4.2 ± 1.9	5.0 ± 2.3	1.1102 r = 0.9936	0.472 -0.267 to 1.210	1.1787 r = 0.9932	0.753 -0.112 to 1.618
4. Inferior	4.2 ± 1.8	3.9 ± 1.6	4.6 ± 2.0	1.1044 r = 0.9944	0.430 -0.136 to 0.995	1.1725 r = 0.9915	0.659 -0.161 to 1.479
5. Inferolateral	4.7 ± 2.0	4.5 ± 1.8	5.4 ± 2.3	1.13 r = 0.9886	0.603 -0.278 to 1.485	1.1999 r = 0.9901	0.871 -0.173 to 1.916
6. Anterolateral	5.2 ± 1.9	5.0 ± 1.7	5.9 ± 2.1	1.1262 r = 0.9883	0.672 -0.050 to 1.394	1.1827 r = 0.9886	0.901 -0.011 to 1.812
Mid							
7. Anterior	5.7 ± 3.0	5.4 ± 2.9	6.4 ± 3.6	1.1413 r = 0.9942	0.720 -0.634 to 2.074	1.2013 r = 0.9952	1.019 -0.533 to 2.570
8. Anteroseptal	4.8 ± 2.8	4.5 ± 2.6	5.3 ± 3.3	1.1159 r = 0.9951	0.495 -0.559 to 1.548	1.1992 r = 0.9932	0.835 -0.602 to 2.271
9. Inferoseptal	5.1 ± 2.4	4.8 ± 2.2	5.6 ± 2.7	1.0944 r = 0.9942	0.459 -0.333 to 1.251	1.1794 r = 0.9895	0.813 -0.405 to 2.031
10. Inferior	4.7 ± 1.6	4.6 ± 1.5	5.3 ± 1.8	1.1218 r = 0.9875	0.584 -0.081 to 1.249	1.1725 r = 0.9878	0.765 -0.076 to 1.606
11. Inferolateral	5.1 ± 1.8	4.9 ± 1.7	5.8 ± 2.2	1.1441 r = 0.9816	0.724 -0.278 to 1.725	1.2061 r = 0.9880	0.964 -0.139 to 2.068
12. Anterolateral	5.7 ± 2.1	5.5 ± 1.9	6.5 ± 2.4	1.1391 r = 0.9852	0.789 -0.222 to 1.799	1.1968 r = 0.9911	1.025 -0.146 to 2.195
Apical							
13. Anterior	4.7 ± 3.1	4.6 ± 3.1	5.5 ± 3.8	1.1794 r = 0.9952	0.757 -0.760 to 2.274	1.2061 r = 0.9952	0.907 -0.627 to 2.441
14. Septal	3.7 ± 2.1	3.4 ± 1.9	4.1 ± 2.4	1.1176 r = 0.9935	0.386 -0.441 to 1.213	1.2093 r = 0.9905	0.644 -0.556 to 1.843
15. Inferior	3.6 ± 1.4	3.4 ± 1.2	4.0 ± 1.6	1.1105 r = 0.9888	0.381 -0.227 to 0.989	1.1846 r = 0.9842	0.570 -0.326 to 1.465

Table 3. continued

¹⁸ F viability segments	Average contrast			HD-PET vs 2D		HD-PET vs 3D	
	2D	3D	HD-PET	Lin. reg. (slope and r)	Bland-Altman (bias, 95%LOAs)	Lin. reg. (slope and r)	Bland-Altman (bias, 95%LOAs)
16. Lateral	4.4 ± 1.9	4.3 ± 1.8	5.1 ± 2.4	1.1619 r = 0.9900	0.690 -0.295 to 1.675	1.2121 r = 0.9893	0.848 -0.354 to 2.050
Apex							
17. Apex	3.0 ± 1.8	2.9 ± 1.6	3.4 ± 2.2	1.1485 r = 0.9930	0.405 -0.426 to 1.235	1.2198 r = 0.9899	0.535 -0.621 to 1.691

Contrast per segment for 2D- and 3D-AWOSEM and HD-PET. Linear regression slope and correlation, and Bland-Altman bias and 95% limits of agreement (LOA) are also given for each segment.

and CNR comparisons in static and gated images for all reconstruction methods are shown in Figures 5, 6 and 7.

Contrast between defect and maximum uptake in myocardium. We found that for both viability and perfusion patients, the maximum uptake-to-defect contrast was significantly increased with HD-PET ($P < .05$). All results are given in Table 2.

Myocardial wall thickness and volume. In the static viability studies, we found significant decrease in the wall thickness and volume with the use of HD-PET. The average measured wall thickness (volume) changed from 18.2 ± 3.2 mm (192.8 ± 56.2 mL) for 2D-AWOSEM and 18.0 ± 3.3 mm (189.6 ± 54.3 mL) for 3D-AWOSEM, to 16.2 ± 3.5 mm (181.3 ± 53.8 mL) for HD-PET (all $P < .05$). In the static perfusion studies, we found a significant decrease in the wall thickness with HD-PET (21.8 ± 2.3 mm) as compared to 3D-AWOSEM (22.9 ± 2.6 mm) but not as compared to 2D-AWOSEM (22.3 ± 2.6 mm). The measured wall volume was 150.2 ± 36.8 for 2D-AWOSEM, 151.5 ± 36.4 for 3D-AWOSEM and 149.4 ± 37.7 for HD-PET (all $P = NS$).

Ejection fraction, wall motion and wall thickening. We found no statistically significant differences in the ejection fraction (EF) measured on gated HD-PET viability and perfusion images compared to the gated images reconstructed with standard methods. The average EF changes HD-PET studies in the 14 viability patients were $-3.5\% \pm 11.8\%$ as compared to 2D-AWOSEM and $-2.7\% \pm 13.1\%$ as compared to 3D-AWOSEM (both $p = NS$). In the 15 perfusion patients, the EF changes for HD-PET were $5.2\% \pm 17\%$ for 2D-AWOSEM and $2.8\% \pm 12.3\%$ for 3D-AWOSEM (both $P = NS$). None of the 17 AHA segments show significant changes in the wall motion or wall thickening estimated by QPET. The average global wall motion (thickening) for the 14 viability patients was 3.68 ± 1.02 mm ($24.7\% \pm 11.9\%$) for 2D-AWOSEM, 3.63 ± 0.99 mm ($26.3\% \pm 13.6\%$) for 3D-AWOSEM and 3.57 ± 1.14 mm ($24.3\% \pm 15.3\%$) for HD-PET (all $P = NS$).

DISCUSSION

HD-PET modeling of the 3D detector spatial response during the reconstruction step is designed to better control the noise in the reconstructed images in general.⁵ In this work, we have shown that HD-PET improves significantly the technical image quality of cardiac studies. The noise, contrast and wall thickness were improved in phantom, viability studies and perfusion studies (static and gated).

The change in contrast and wall thickness can in most part be explained by the improved spatial

Table 4. ^{82}Rb perfusion studies

^{82}Rb perfusion segments	Average contrast			HD-PET vs 2D		HD-PET vs 3D	
	2D	3D	HD-PET	Lin. reg. (slope and <i>r</i>)	Bland-Altman (bias, 95%LOAs)	Lin. reg. (slope and <i>r</i>)	Bland-Altman (bias, 95%LOAs)
Basal							
1. Anterior	2.6 ± 0.6	2.5 ± 0.5	2.7 ± 0.6	1.0389 <i>r</i> = 0.9650	0.098 -0.230 to 0.426	1.0867 <i>r</i> = 0.9877	0.199 -0.063 to 0.462
2. Anteroseptal	2.2 ± 0.5	2.1 ± 0.4	2.3 ± 0.5	1.0286 <i>r</i> = 0.8934	0.074 -0.351 to 0.500	1.085 <i>r</i> = 0.9786	0.173 -0.067 to 0.412
3. Inferoseptal	2.1 ± 0.5	2.0 ± 0.3	2.2 ± 0.4	1.0054 <i>r</i> = 0.9047	0.027 -0.332 to 0.387	1.0748 <i>r</i> = 0.9816	0.142 -0.058 to 0.342
4. Inferior	2.2 ± 0.5	2.1 ± 0.4	2.2 ± 0.5	1.0276 <i>r</i> = 0.9578	0.069 -0.222 to 0.360	1.0754 <i>r</i> = 0.9904	0.147 -0.044 to 0.339
5. Inferolateral	2.3 ± 0.4	2.1 ± 0.4	2.3 ± 0.4	1.0164 <i>r</i> = 0.8997	0.048 -0.324 to 0.419	1.088 <i>r</i> = 0.9882	0.183 0.014-0.351
6. Anterolateral	2.4 ± 0.4	2.3 ± 0.4	2.5 ± 0.5	1.026 <i>r</i> = 0.9004	0.068 -0.324 to 0.459	1.0845 <i>r</i> = 0.9779	0.183 -0.051 to 0.416
Mid							
7. Anterior	2.9 ± 0.6	2.7 ± 0.6	3.0 ± 0.6	1.0394 <i>r</i> = 0.9391	0.114 -0.321 to 0.549	1.0865 <i>r</i> = 0.9937	0.231 0.027-0.435
8. Anteroseptal	2.7 ± 0.5	2.6 ± 0.5	2.8 ± 0.5	1.0342 <i>r</i> = 0.8945	0.102 -0.367 to 0.571	1.0902 <i>r</i> = 0.9907	0.232 0.045-0.418
9. Inferoseptal	2.7 ± 0.5	2.5 ± 0.4	2.7 ± 0.5	1.0265 <i>r</i> = 0.8824	0.081 -0.352 to 0.514	1.0873 <i>r</i> = 0.9890	0.214 0.027-0.400
10. Inferior	2.5 ± 0.6	2.4 ± 0.5	2.6 ± 0.6	1.0322 <i>r</i> = 0.9490	0.087 -0.297 to 0.470	1.0782 <i>r</i> = 0.9923	0.182 -0.030 to 0.393
11. Inferolateral	2.5 ± 0.5	2.4 ± 0.5	2.6 ± 0.6	1.0425 <i>r</i> = 0.9292	0.102 -0.330 to 0.533	1.0894 <i>r</i> = 0.9937	0.211 0.022-0.400
12. Anterolateral	2.8 ± 0.4	2.7 ± 0.4	3.0 ± 0.5	1.0507 <i>r</i> = 0.9104	0.142 -0.273 to 0.557	1.0839 <i>r</i> = 0.9916	0.224 0.049-0.399
Apical							
13. Anterior	2.6 ± 0.5	2.6 ± 0.5	2.8 ± 0.6	1.0639 <i>r</i> = 0.9512	0.171 -0.167 to 0.509	1.098 <i>r</i> = 0.9908	0.244 0.035-0.453
14. Septal	2.5 ± 0.4	2.4 ± 0.4	2.6 ± 0.5	1.0374 <i>r</i> = 0.8874	0.099 -0.330 to 0.529	1.0926 <i>r</i> = 0.9899	0.218 0.045-0.391
15. Inferior	2.5 ± 0.5	2.4 ± 0.5	2.6 ± 0.6	1.0461 <i>r</i> = 0.9527	0.119 -0.205 to 0.443	1.0861 <i>r</i> = 0.9920	0.197 0.000-0.394

Table 4. continued

⁸² Rb perfusion segments	Average contrast			HD-PET vs 2D		HD-PET vs 3D	
	2D	3D	HD-PET	Lin. reg. (slope and r)	Bland-Altman (bias, 95%LOAs)	Lin. reg. (slope and r)	Bland-Altman (bias, 95%LOAs)
16. Lateral	2.5 ± 0.5	2.4 ± 0.4	2.6 ± 0.5	1.059 r = 0.9230	0.150 -0.232 to 0.531	1.0887 r = 0.9957	0.209 0.060-0.358
Apex							
17. Apex	2.2 ± 0.4	2.2 ± 0.4	2.4 ± 0.5	1.0623 r = 0.9367	0.140 -0.195 to 0.475	1.0991 r = 0.9898	0.210 0.026-0.393

Contrast per segment for 2D- and 3D-AWOSEM and HD-PET. Linear regression slope and correlation, and Bland-Altman bias and 95% limits of agreement (LOA) are also given for each segment.

resolution of HD-PET. 2D- and 3D-AWOSEM achieve at best 4.7 mm spatial resolution in reconstructed PET images in the center of the FOV.¹⁷ The spatial resolution of these standard reconstruction techniques also degrades in regions of interest off the center of the FOV (to 5.6 mm at 10 cm from the center of the FOV and to 7.2 mm at 20 cm off the center) while HD-PET provides an almost uniform resolution over the entire FOV.⁵ Partial volume effects (PVE) greatly affect the accuracy of cardiac PET images. The main source of PVE is the spatial resolution in the reconstructed images. The relatively low image resolution compared to the myocardial wall thickness leads to an underestimation of the tracer concentration in the myocardium wall.¹⁸ By improving the spatial resolution, HD-PET limits the impact of the PVE and provides higher contrast images as compared to the standard reconstruction methods. The smaller contrast improvement with HD-PET for the perfusion studies as compared to the viability studies is likely due to the larger positron range of ⁸²Rb (4.1 mm vs 0.6 mm for ¹⁸F)¹⁹ and consequently poor image quality of the perfusion studies. However, perfusion studies with new ¹⁸F based perfusion agent are being introduced²⁰ and these studies will likely benefit more from improved image resolution similar to the viability studies.

The maximum defect contrast, related to the severity of the defect, increased with HD-PET in both phantom and patients images. We also have shown that in phantom experiments, defects closer to the physical defect sizes are observed with HD-PET as compared to 2D- and 3D-AWOSEM. In routine clinical cardiac imaging, it is therefore reasonable to expect that defect extent and severity will be changed with the use HD-PET. The improved spatial resolution and noise characteristics of HD-PET will likely allow detection of smaller defects, consequently increasing sensitivity and accuracy of diagnostics. However, this remains to be evaluated in clinical studies.

HD-PET could become the preferred reconstruction technique when doing low statistics acquisitions such as dual (cardiac and respiratory) gating studies due to better control of noise as demonstrated by the improved CNR.

The reconstruction time is significantly increased with HD-PET. However, based on our results, there are significant improvements in image quality and defect definition, which may be worth the extra reconstruction time. It should be noted that faster computers can be utilized for these reconstructions and it is likely that the speed of these advanced reconstruction will be rapidly improved in the near future.

We did not find any significant changes in the ejection fraction, wall motion or thickening estimated by

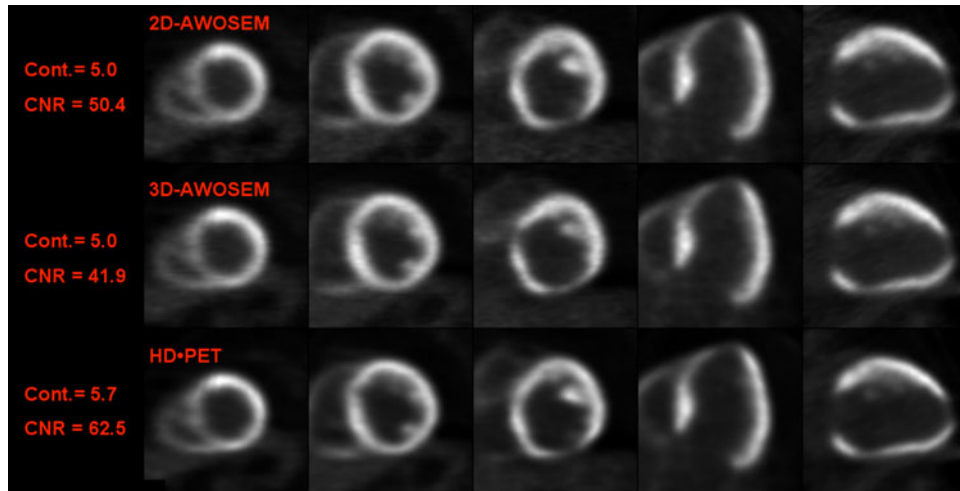


Figure 5. Comparison of all reconstruction methods for cardiac ^{18}F -FDG viability images in a 56-year-old male patient (weight, 77 kg [170 lb]; body mass index 27.6). The figure shows short axis, vertical and horizontal long axis views of 2-mm Gauss filtered static images reconstructed with 2D-AWOSEM, 3D-AWOSEM and HD-PET.

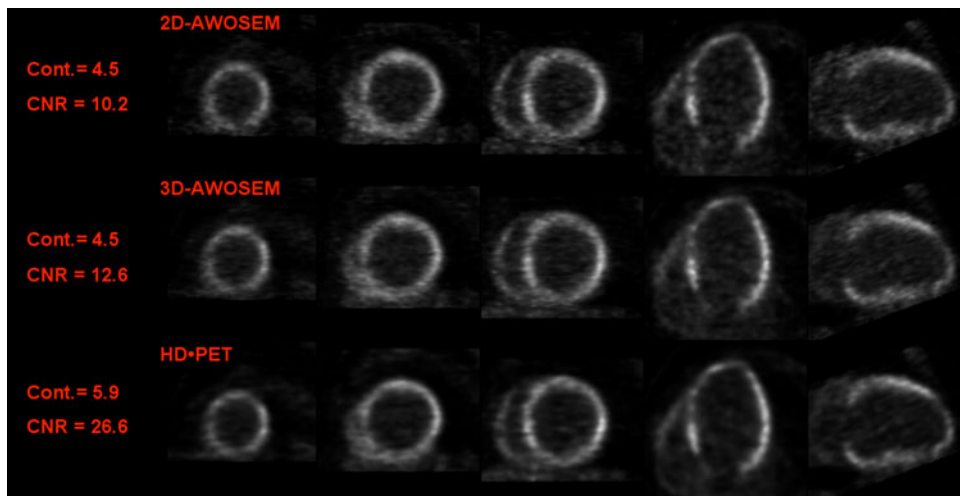


Figure 6. Example of image quality in gated viability study reconstructed with HD-PET. A 51-year-old male patient (weight, 82 kg [181 lb]; body mass index 29.2) referred for ^{18}F -FDG cardiac viability assessment. The figure shows short axis, vertical and horizontal long axis views of 2-mm Gauss filtered end-diastolic images reconstructed with 2D-AWOSEM, 3D-AWOSEM and HD-PET.

QPET for HD-PET as compared to the two other techniques. The ejection fraction is calculated using the difference between two automatically detected volumes (end-diastole ED and end-systole ES ones), both of which are affected by PVE in the same proportions. QPET uses automatically detected endocardial and pericardial contours for the wall motion (points at mid way) and thickening (endo- and pericardial points)

evaluation. In all cases, the improvement with HD-PET is canceled out by the estimation method. Therefore, we did not observe global changes; however, it is possible that wall thickening could be depicted more accurately in individual cases but this remains to be validated.

Because of the better control of noise as demonstrated by the improved CNR, HD-PET could become the preferred reconstruction technique when doing low

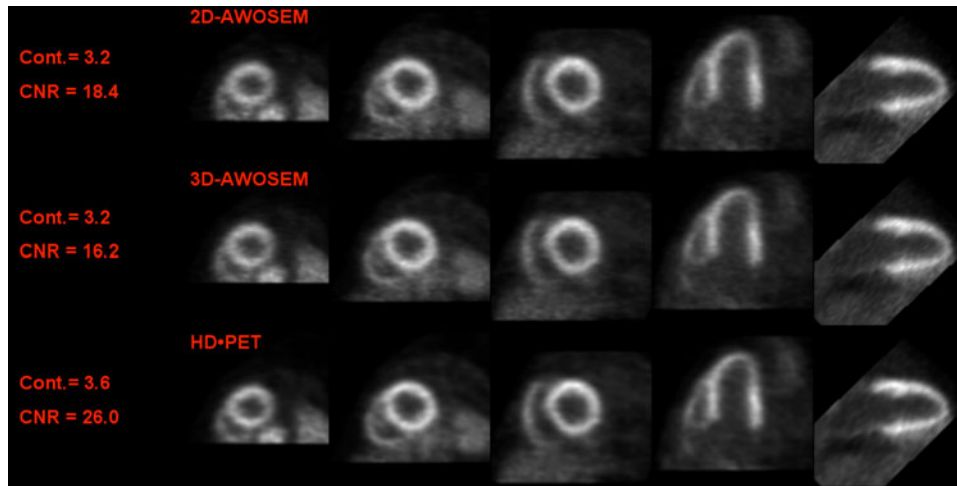


Figure 7. Example of image quality in static perfusion patient data reconstructed with HD-PET. A 59-year-old female patient (weight, 52 kg [115 lb]; body mass index 13.6) referred for ^{82}Rb cardiac perfusion assessment. The figure shows short axis, vertical and horizontal long axis views of 2-mm Gauss filtered images reconstructed with 2D-AWOSEM, 3D-AWOSEM and HD-PET.

statistics acquisitions such as dual (cardiac and respiratory) gating studies. Such studies have the potential to improve the spatial resolution of images but they use a large number of gates and are subjected to a high noise in each gate, diminishing the diagnostic potential of the images.

Study Limitations

No moving phantom (cardiac and respiratory motion) was used in this study. There was no gold standard for the clinical wall thickness or defect size and no angiography data to confirm CAD. Our patient population had a limited range of BMI. Only one patient in our cohort had a BMI higher than 40. In this patient, the contrast was increased by 27.1% and the CNR by a factor 2.0 compared to regular reconstruction techniques. A study with high BMI patients is needed to prove that our results can be extrapolated. We did not apply “Motion Frozen” processing method²¹ to gated HD-PET images which could have further enhanced image quality.

CONCLUSIONS

Our work on both phantom and patient cardiac studies showed that HD-PET significantly improved defect definition, image resolution, contrast and contrast-to-noise and provided equivalent functional quantitative information compared to standard reconstruction techniques. This improved technical quality

could lead to improved performance of cardiac PET/CT. Further evaluation of the clinical impact of HD-PET on cardiac imaging would appear to be warranted.

Acknowledgments

The authors thank Jimmy Fermin and Brandi N. Huber from Cedars-Sinai Medical Center for their help with the PET acquisition, Heidi Gransar for her help with the statistical analysis and Michael Casey from Siemens Healthcare for his help with the setting up of the High Definition.

References

1. Manjeshwar R, Ross S, Iatrou M, Deller T, Stearns C, Res G, et al. Fully 3D PET iterative reconstruction using distance-driven projectors and native scanner geometry. *IEEE Nucl Sci Symp Conf Rec* 2006;5:2804-7.
2. Chang G, Pan T, Qiao F, Clark J Jr, Mawlawi O. Comparison between two super-resolution implementations in PET imaging. *Med Phys* 2009;36:1370.
3. Kennedy J, Israel O, Frenkel A, Bar-Shalom R, Azhari H. Super-resolution in PET imaging. *IEEE Trans Med Imaging* 2006;25:137-47.
4. De Bernardi E, Mazzoli M, Zito F, Baselli G. Resolution recovery in PET during AWOSEM reconstruction: A performance evaluation study. *IEEE Trans Nucl Sci* 2007;54:1626-38.
5. Panin VY, Kehren F, Michel C, Casey M. Fully 3-D PET reconstruction with system matrix derived from point source measurements. *IEEE Trans Med Imaging* 2006;25:907-21.
6. Kudo T. Metabolic imaging using PET. *Eur J Nucl Med Mol Imaging* 2007;34:49-61.
7. Di Carli M, Dorbala S, Meserve J, El Fakhri G, Sitek A, Moore S. Clinical myocardial perfusion PET/CT. *J Nucl Med* 2007;48:783.
8. Jonsson C, Odh R, Schnell PO, Larsson SA. A comparison of the imaging properties of a 3-and 4-ring biograph PET scanner using a

- novel extended NEMA phantom. *IEEE Nucl Sci Symp Conf Rec* 2007;4:2865-7.
9. Townsend D, Jakoby B, Long M, Carr C, Hubner K, Guglielmo C, et al. Performance and clinical workflow of a new combined PET/CT scanner. *J Nucl Med* 2007;48:437P.
 10. Watson C, Hayden C, Casey M, Hamill J, Bendriem B. Prompt gamma correction for improved quantification in ^{82}Rb PET. *J Nucl Med* 2008;49:64P.
 11. Hudson HM, Larkin RS. Accelerated image reconstruction using ordered subsets of projection data. *IEEE Trans Med Imaging* 1994;13:601-9.
 12. Slomka P, Dorbala S, Berman D, Gerlach J, Germano G, DiCarli M. Automated quantification and normal limits for myocardial perfusion stress/rest Rb-82 PET/CT. *J Nucl Med* 2009;50:216P.
 13. Cerqueira M, Weissman N, Dilsizian V, Jacobs A, Kaul S, Laskey W, et al. Standardized myocardial segmentation and nomenclature for tomographic imaging of the heart a statement for healthcare professionals from the Cardiac Imaging Committee of the Council on Clinical Cardiology of the American Heart Association 2002. p. 539-42.
 14. Slomka PJ, Nishina H, Berman DS, Kang X, Friedman JD, Hayes SW, et al. Automatic quantification of myocardial perfusion stress-rest change: A new measure of ischemia. *J Nucl Med* 2004;45:183-91.
 15. Slomka P, Germano G, Kavanagh P, Javadi M, Berman D, Bengel F. Evaluation of a new automatic algorithm for quantification of ECG-gated ^{82}Rb cardiac PET. *J Nucl Med* 2009;50:217P.
 16. Kadrmas D, Casey M, Conti M, Jakoby B, Lois C, Townsend D. Impact of time-of-flight on PET tumor detection. *J Nucl Med* 2009;50:1315.
 17. Conti M, Bendriem B, Casey M, Eriksson L, Jakoby B, Jones WF, et al. Performance of a high sensitivity PET scanner based on LSO panel detectors. *IEEE Trans Nucl Sci* 2006;53.
 18. Hoffman EJ, Huang SC, Phelps ME. Quantitation in positron emission computed tomography: 1. Effect of object size. *J Comput Assist Tomogr* 1979;3:299.
 19. Sanchez-Crespo A, Andreo P, Larsson S. Positron flight in human tissues and its influence on PET image spatial resolution. *Eur J Nucl Med Mol Imaging* 2004;31:44-51.
 20. Maddahi J, Schiepers C, Czernin J, Huang H, Schelbert H, Wijatyk A, et al. First human study of BMS747158, a novel F-18 labeled tracer for myocardial perfusion imaging. *J Nucl Med* 2008;49:70P.
 21. Slomka PJ, Nishina H, Berman DS, Kang X, Akincioglu C, Friedman JD, et al. "Motion-Frozen" display and quantification of myocardial perfusion. *J Nucl Med* 2004;45:1128-34.